High Performance Microshield Line Components

Thomas M. Weller, *Student Member, IEEE*, Linda P. B. Katehi, *Fellow, IEEE*, and Gabriel M. Rebeiz, *Senior Member, IEEE*

Abstract— **Several millimeter-wave passive components have been fabricated using the microshield transmission line geometry, and their performance is presented herein. Microshield is a quasi-planar, half-shielded design which uses a thin dielectric membrane (1.5 μm) to support the conducting lines. This approach provides a nearly homogeneous, air-filled environment and thus allows extremely broad-band TEM operation. This paper examines the conductor loss and effective dielectric constant of microshield lines and presents results on transitions to conventional coplanar waveguide, right-angle bends, different stub configurations, and lowpass and bandpass filters. Experimental data is provided along with numerical results derived from an integral equation method. The microshield line is shown to be very suitable for high performance millimeter- and submillimeter-wave applications.**

I. Introduction

THE microshield line was introduced in 1991 as an alternative transmission medium to coplanar waveguide for millimeter- and submillimeter-wave applications [1]. It is a partially shielded, quasi-planar transmission line in which the center conductor and upper ground planes are surrounded by air and supported by a 1.5-μm-thick dielectric membrane, as shown in Figs. 1 and 2. This configuration allows single-mode, TEM wave propagation over a very broad bandwidth with minimal dispersion and zero dielectric loss. Furthermore, the metallized lower shielding cavity minimizes signal cross-talk between adjacent lines and eliminates radiation into parasitic substrate modes. Another advantage of microshield relates to the fact that parasitic effects associated with circuit discontinuities decrease with the dielectric constant of the substrate. Thus, the membrane-supported geometry offers the optimum conditions for making circuit performance less susceptible to frequency dependent phenomena such as end-effects, thereby simplifying circuit design. A description of these and other advantages of the microshield geometry can be found in previous communications [2]–[4], along with a summary of the fabrication process.

The objective of this paper is to present results from a detailed study which emphasizes microshield circuit design and measurement in the 10–40 GHz frequency range. An important part of the project has been the development of a good transition between the microshield line and the measurement probe contact pads, which must be printed on the surrounding high-resistivity silicon substrate for mechanical support. This transition is covered in detail in Section II. The conductor loss of microshield, discussed in Section III, has been measured on lines of different aspect ratios and values as low as 0.03 dB/mm at 35 GHz have been obtained. These results demonstrate the potential for low-loss, millimeter-wave interconnect lines and passive circuit elements. The data are also consistent with the findings from recent opto-electronic sampling experiments, in which low-loss signal propagation on membrane lines has been measured up to 1 THz, well beyond the upper frequency limits of similar GaAs and quartz supported lines [5]. In Section IV, some of the advantages offered by the very low effective dielectric constant of the microshield line are covered. The performance of several microshield circuits such as transitions to CPW lines, right-

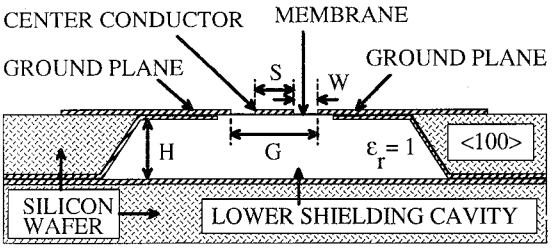

Fig. 1. The microshield transmission line geometry (not to scale). The cross-hatched lines indicate metallization, which is typically 1–2 μm thick.

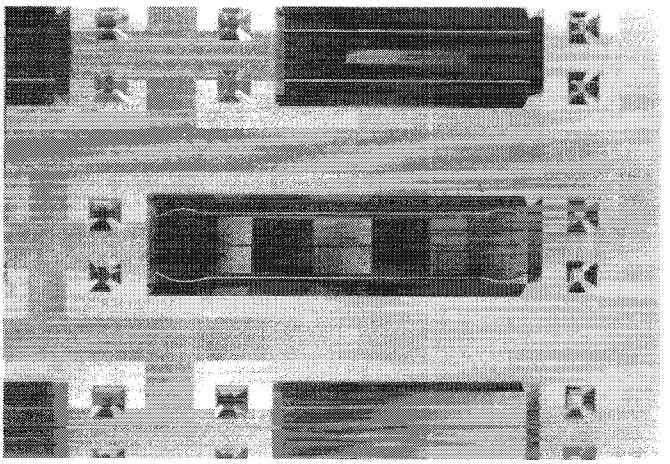

Fig. 2. Photograph of the backside of a wafer, shown with the ground plane removed. The circuit in the center is a five-section stepped-impedance lowpass filter (see Fig. 15).

Manuscript received February 15, 1994; revised July 11, 1994. This work was supported by the NASA Center for Space Terahertz Technology and the Office of Naval Research.

The authors are with the NASA/Center for Space Terahertz Technology, University of Michigan, Ann Arbor, MI 48109-2122 USA.

IEEE Log Number 9407453.

angle bends, series stubs, lowpass filters, and a bandpass filter is presented in Section V.

In addition to measured data, numerical results from a full-wave analysis are provided as a validation of the measurements and also as a means to predict the performance beyond the 40-GHz limit of the measurement setup. The theory is based on a space domain integral equation (SDIE), similar to that described in [6] but capable of analyzing non-shielded geometries. The SDIE is derived by replacing the slots in the metallization by fictitious metal surfaces, and then imposing magnetic currents on the surfaces which must satisfy the field continuity conditions. The method of moments is used to discretize the integral equation and solve for the magnetic currents, or electric fields, in the slots, from which the scattering parameters can be determined. It is assumed that all conductors are infinitely thin and perfectly conducting, and that the shape of the lower shielding cavity is rectangular. In addition, the effect of the thin membrane layer is approximated by assuming that the lower cavity is homogeneously filled with a material which has a dielectric constant slightly greater than 1 (Section IV).

This paper shows that characteristics of the microshield line are well-suited for specialized millimeter-wave and submillimeter-wave applications. Integrating the thin dielectric membrane on silicon or GaAs substrates requires additional steps in the fabrication process, but in many cases this is offset by eliminating the procedures for air-bridges and substrate thinning. Furthermore, the circuit yield is very high, exceeding 95% in a research laboratory, and the substrate etch can be one of the last steps in the process, thereby increasing yield. These factors, combined with the very broad-band, low-loss performance, make microshield a viable transmission line option for systems operating at mm-wave frequencies.

II. Measurement and System Calibration

In this section the measurement setup is described along with some details regarding the line standards needed for calibration. The measurements are made using a microwave probe station and an HP 8510B vector network analyzer. Since the membranes cannot withstand repeated probe contact, the contact pads are short sections of grounded coplanar waveguide (GCPW) on the silicon substrate, and a transition is made onto the microshield line. A one-tier TRL technique [7] is utilized to calibrate to reference planes which are on the microshield line.

It was found that the geometry of the probe contact pads and the transition section have an important effect on the quality of the calibration. The initial design, shown in Fig. 3, consisted of 55 Ω GCPW contact pads followed by a 735-μm-long GCPW impedance matching section. This configuration was intended to act as a low-loss transition to the 75 Ω microshield line, the effects of which could be removed with the TRL calibration. Even though the non-calibrated return loss from the thru and delay lines was consistently better than 12 dB, the performance of this design was rather poor and repeatability was difficult to achieve. Typical results for the calibrated insertion loss of a microshield delay line are also shown in Fig. 3.

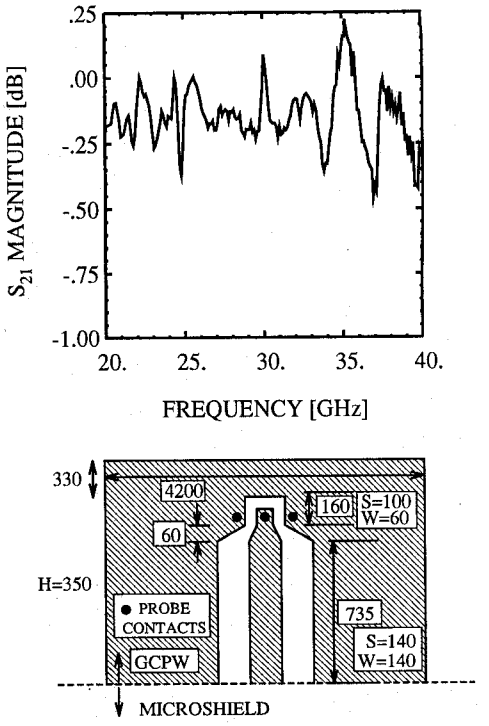

Fig. 3. A transition from the CPW microwave probes to the microshield line, and the measured S_{21} of a microshield delay line using this design. All dimensions are in microns.

The cause of the measurement errors is the leakage of power into undesired substrate modes along the length of grounded CPW line, which cannot be accounted for correctly using the standard HP 8510B TRL calibration software. The discontinuities at the probe contact pads, impedance steps, and the end of the microshield cavity are all possible sources of excitation for undesired parallel plate modes and TM_n and TE_n surface waves [8]–[16]. Also, as reported in [12], the finite lateral extent of the ground planes can result in distinctly predictable resonances in GCPW delay lines.

The leakage mechanism associated with the transition in Fig. 3 exhibits a consistent structure across the 20–40 GHz band, apart from the sharp resonance seen around 35 GHz. The circuit dimensions suggest that the primary problem is leakage into the TEM parallel plate mode [10]. Different authors have shown that the ground plane spacing $(S + 2W)$must be kept small compared to the ground plane width, G, and the substrate height, H, in order to maintain propagation in the CPW-like mode [13], [15], [16]. Furthermore, since the power leakage increases with distance, a shorter length of GCPW between the probe contact pads and the microshield line can also reduce this problem. Finally, leaky modes may be eliminated by integrating metallized cavities in the back of the substrate near the probe contact points (see Fig. 2).

These three modifications were implemented into the transition design shown in Fig. 4, and the significant improvement in the calibration is demonstrated in the same figure. In a later design, the ripple near 36 GHz was reduced by completely eliminating the 300 μm length of GCPW line.

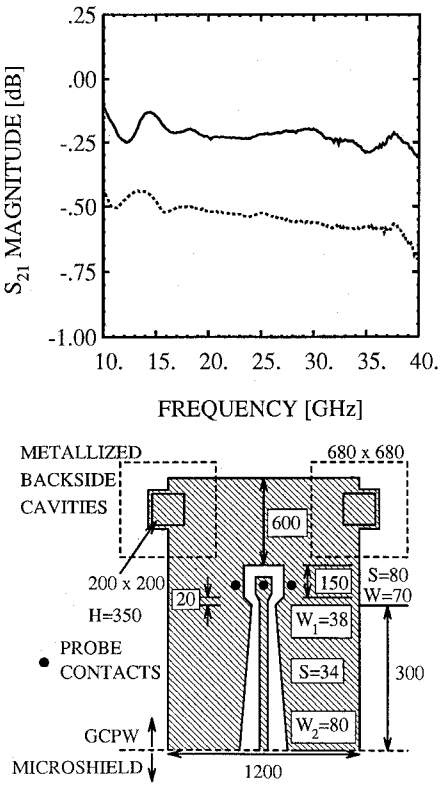

Fig. 4. Measured S_{21} of two microshield delay lines of different length, using the modified transition from the CPW probes. The cavities are etched from the backside of the wafer and are pyramidal in shape; the dotted line is the cavity size at the bottom of the wafer. All dimensions are in microns.

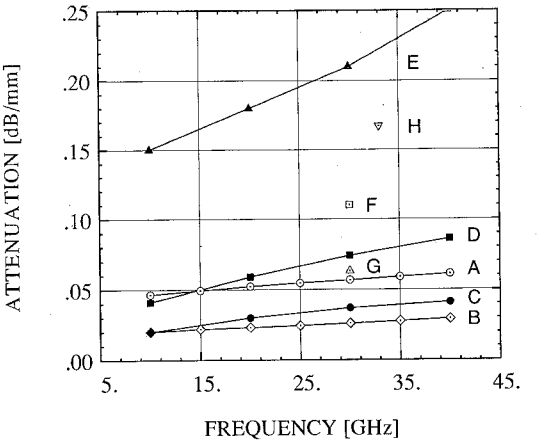

Curve	Line	ϵ_r	Substr	S	W	H	t	Z_O Ω	Data	Ref.
A	μshield	1.0	Air	250	25	355	1.2	75	Meas	–
B	μshield	1.0	Air	190	55	355	1.2	100	Meas	–
C	CPW	12.8	GaAs	232	84	100	-	50	Calc	18
D	CPW	12.8	GaAs	69	28	100	-	50	Calc	18
E	CPW	12.9	GaAs	88	16	500	1.0	30	Meas	19
F	CPW	12.9	GaAs	250	25	500	1.0	30	Calc	16
G	CPW	4.0	Quartz	250	25	250	1.0	50	Calc	16
H	GCPW	11.7	Si	50	125	355	1.2	73	Meas	–

Fig. 5. Attenuation for microshield and coplanar waveguide lines. S is the center conductor width, W the slot width, H the substrate height, and t the metal thickness (in μm). The width of the lower shielding cavity for the microshield lines is 1800 μm.

III. Attenuation

The attenuation characteristics of the microshield line have been investigated by comparing measured data on different microshield geometries against experimental and theoretical results for coplanar waveguide which are found in the literature [16], [18], [19]. At low frequencies, the two types of lines are expected to perform equally well, since dielectric and radiative losses are relatively small and attenuation is therefore dominated by conductor loss. At higher frequencies, however, the microshield line gains an increasing advantage since it has essentialy zero dielectric loss and does not radiate energy into the substrate, unlike a substrate-supported CPW line. This characteristic has been verified by recent electro-optic sampling experiments, which provided attenuation data on membrane-supported lines up to 1000 GHz [5].

The comparison between the microshield and CPW attenuation is shown in Fig. 5. The microshield data in curves A and B was generated by averaging the measured insertion loss for several lines with lengths between 2.3 mm and 8.5 mm, while the GCPW data of point H was taken from measurements of a microshield-to-GCPW transition on a high-resistivity silicon wafer ($\rho >$ 2000 Ω-cm). The CPW curves which are shown for comparison were chosen either because the dimensions are similar to the microshield lines (curves C, F, and G) or to illustrate the effects of reducing the line geometry (curves D, E). All pertinent geometrical parameters for the CPW and microshield examples are given in the table beneath the figure, and it is noted that the conductor thickness is only about 2 skin depths at 25 GHz for all but two cases.[1]

Some aspects of the information shown in Fig. 5 deserve comment. The first point is that the results for the microshield lines are consistent with the CPW loss behavior outlined in [17] by Jackson; namely, for a constant ground plane separation, an aspect ratio $(S/S + 2W)$ of 0.83 (curve A) gives much higher loss than an aspect ratio of 0.63 (curve B). A second point relates to a comparison between the CPW and microshield data in terms of loss per electrical length, as the wavelength in the air dielectric is about 2.5 times longer than in GaAs and about 1.5 times longer than in quartz. The *calculated* loss for CPW in points F and G is about 0.1 dB/λ_g lower than the *measured* loss in curve A for the microshield line, which has identical center conductor and slot widths. This is a relatively small difference, however, some of which can be explained by errors in the measured and/or theoretical data. The results presented here confirm that the microshield line is free from unexpected or excessive conductor-loss mechanisms, and has performance which is comparable to conventional substrate-supported coplanar waveguide at lower frequencies. Furthermore, the absence of dielectric-related loss and the ability to maintain non-dispersive, single-mode propagation over a very broad bandwidth lead to low attenuation well into the millimeter-wave frequencies.

IV. Advantages of an Air Substrate

Due to the air substrate of the microshield line, the effective dielectric constant, $\epsilon_{r,\text{eff}}$, is very close to 1. Because of

[1] The technique used in [18] assumes zero conductor thickness.

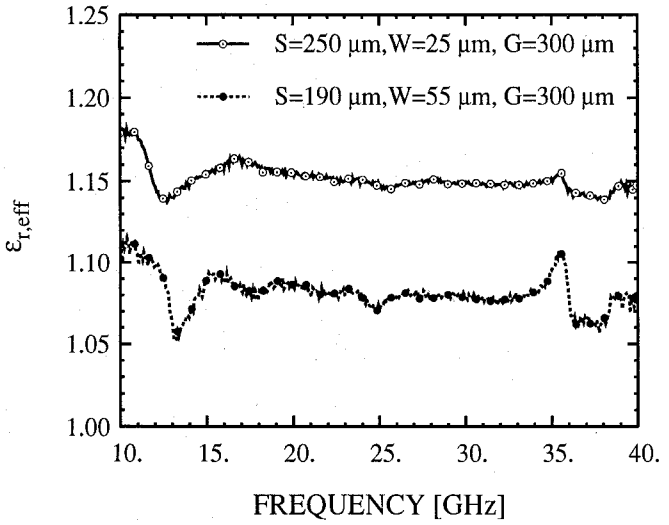

Fig. 6. Measured effective dielectric constant, $\epsilon_{r,eff}$, on two microshield lines with different aspect ratios. The cavity height (H) is 350 μm.

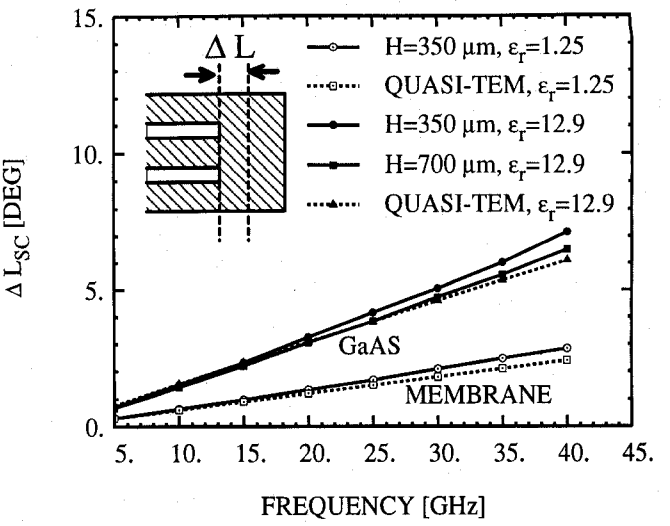

Fig. 7. Effective length extension (in degrees) for a short-end discontinuity on lines with equal aspect ratios of $(S/S + 2W) = 0.33$. The characteristic impedance for the lines are 135 Ω ($\epsilon_r = 1.25$) and 55 Ω ($\epsilon_r = 12.9$). The line parameters are $S = 100$ μm, $W = 100$ μm and the substrate height H is given in the legend.

the membrane, however, $\epsilon_{r,\text{eff}}$ is slightly increased since a fraction of the fields will be contained within the thin dielectric layers. The membrane is a 1.5-μm-thick tri-layer composite of $SiO_2/Si_3N_4/SiO_2$ with constituent thicknesses of approximately 7000 Å/3000Å/4000Å. The dielectric constant of the oxide is 3.9, and that of the nitride is 7.5. As shown in Fig. 6, the measured $\epsilon_{r,\text{eff}}$ changes from around 1.09 to 1.15 as the slot width is reduced from 55 to 25 μm. The increase is a result of greater field confinement in the slot and thus in the membrane, and represents a decrease of nearly 3% in the guided wavelength. This dependence on the slot width is similar to the characteristics of CPW lines on a substrate such as GaAs or quartz [19].

There are several potential advantages of the nearly homogeneous air-dielectric. These include the absence of substrate moding problems, which in turn reduces dispersion and losses due to parasitic radiation. Another advantage is the improved electrical performance of discontinuities such as shorts, opens, steps and bends. As an example, the effective length extension,[2] ΔL_{sc}, of a grounded coplanar short-end on substrates with ϵ_r = 1.25 and 12.9 (GaAs) is shown in Figs. 7 and 8. The value of 1.25 was chosen to yield an *effective* dielectric constant around 1.12, in order to simulate the microshield line. The plots contain theoretical results from the full-wave analysis described in the introduction, and from an expression by Getsinger which is applicable for quasi-TEM lines printed on an infinitely-thick dielectric [20]. In Fig. 7, all lines have $S = W = 100$ μm with substrate heights of 350 and 700 μm, while in Fig. 8, all lines have a characteristic impedance around 65 Ω. Since the end-effect is completely inductive for pure-TEM operation, the *physical* size of the length extension is nearly independent of the dielectric constant. The shorter wavelength in the GaAs substrate, however, makes the extension become longer electrically. A similar argument can be made regarding the performance of coplanar open-ends.

[2]The effective length extension, ΔL_{sc}, is the position at which an ideal short circuit would result in the same impedance seen at the physical end of the line.

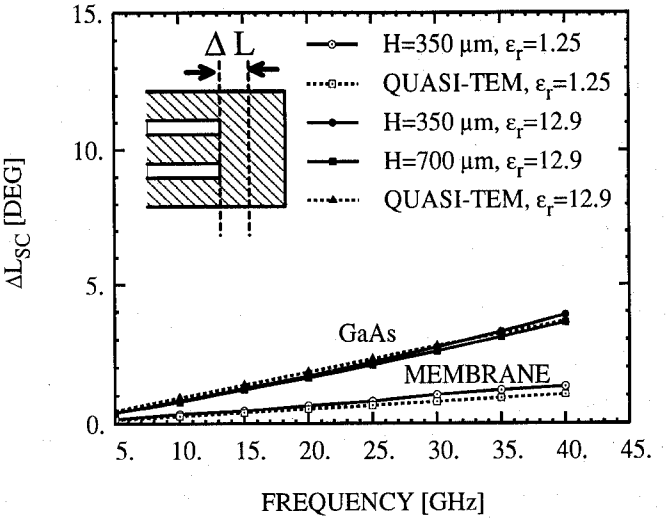

Fig. 8. Effective length extension (in degrees) for a short-end discontinuity on lines with equal characteristic impedance (65 Ω). The parameters are $S = 165$ μm, $W = 10$ μm for the line with $\epsilon_r = 1.25$, and $S = 40$ μm, $W = 67$ μm for the line with $\epsilon_r = 12.9$. The substrate height H is given in the legend.

Under the quasi-TEM conditions, the physical length of the effective length extension, ΔL_{oc}, is roughly independent of ϵ_r, for small values of ΔL_{oc}. Again, this results in an increased electrical length when the substrate dielectric constant is higher, and these end effects can become significant since ΔL_{oc} is typically at least twice as large as ΔL_{sc} [21]. Thus, the air-filled environment of the microshield geometry offers the optimum conditions for making circuit performance less susceptible to this type of frequency dependent behavior.

V. Microshield Circuit Components

A. Transitions to Coplanar Waveguide

An electrically short, low-loss transition between microshield and GCPW is important for measurement calibration

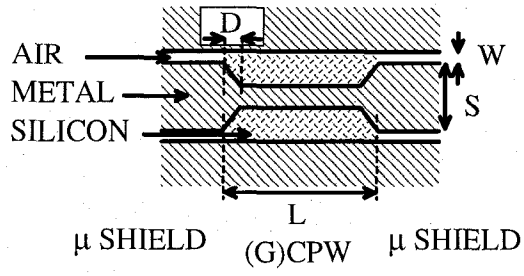

DESIGN	H	L	S	W	D	Z_o Ω
WIDE	350	1460	120	650	0	71
MATCH	350	1460	60	180	0	75
TAPER	350	1460	70	175	140	71

Fig. 9. Three transitions from 75Ω microshield line ($S = 350$ μm, $W = 35$ μm) to CPW and grounded CPW. The dimensions for the GCPW lines are given in the table in microns, and the characteristic impedance values are for the grounded CPW configuration (i.e. with a lower ground plane).

purposes and for applications which could integrate circuit components configured in both types of lines. Furthermore, although quasi-optical and waveguide probe [22] techniques can be used to couple power into or out of a microshield circuit, typical applications will most likely utilize transmission lines printed on a solid substrate to provide mechanical strength at the connection.

It has been found that the similarities of the field configurations in CPW and microshield make broad band, low-loss transitions quite easy to achieve [3], despite the large difference in the dielectric constants of the transmission media. Although a rigorous optimization has not been conducted, designs based on a simple matching of quasi-static characteristic impedance values have demonstrated very good performance up to 40 GHz. Three designs are given in Fig. 9; the 'wide' design has slot widths which are nearly twice the substrate height, and thus will propagate a mode which is similar to that of microstrip, whereas the 'match' and 'taper' designs have narrower slots, leading to propagation of a CPW-like mode. The measured data on these transitions is shown in Fig. 10 and the lower plot shows that a return loss below 20 dB across the entire band has been obtained. For the CPW curves, the ground plane beneath the transition section was removed. Also, the noise in the data is due to the calibration, since the original probe-to-microshield transition was used for these measurements (Fig. 3).

The effect of a field mismatch between the microshield and GCPW lines is evident by comparing the 'wide' and 'match' GCPW designs, which have a similar characteristic impedance but different configurations of the electromagnetic fields. As mentioned, the 'match' design, like the microshield, will have a primarily CPW-like mode since the fields will tend to concentrate in the narrow slots. The slot widths in the 'wide' design, however, lead to propagation in more of a microstrip-like mode since there is greater influence from the lower ground plane. This influence can be examined by computing the change in the characteristic impedance as the substrate height (H) is varied. If H goes from 350 μm, as used in the current lines, to 1 cm, the changes in Z_0 for the

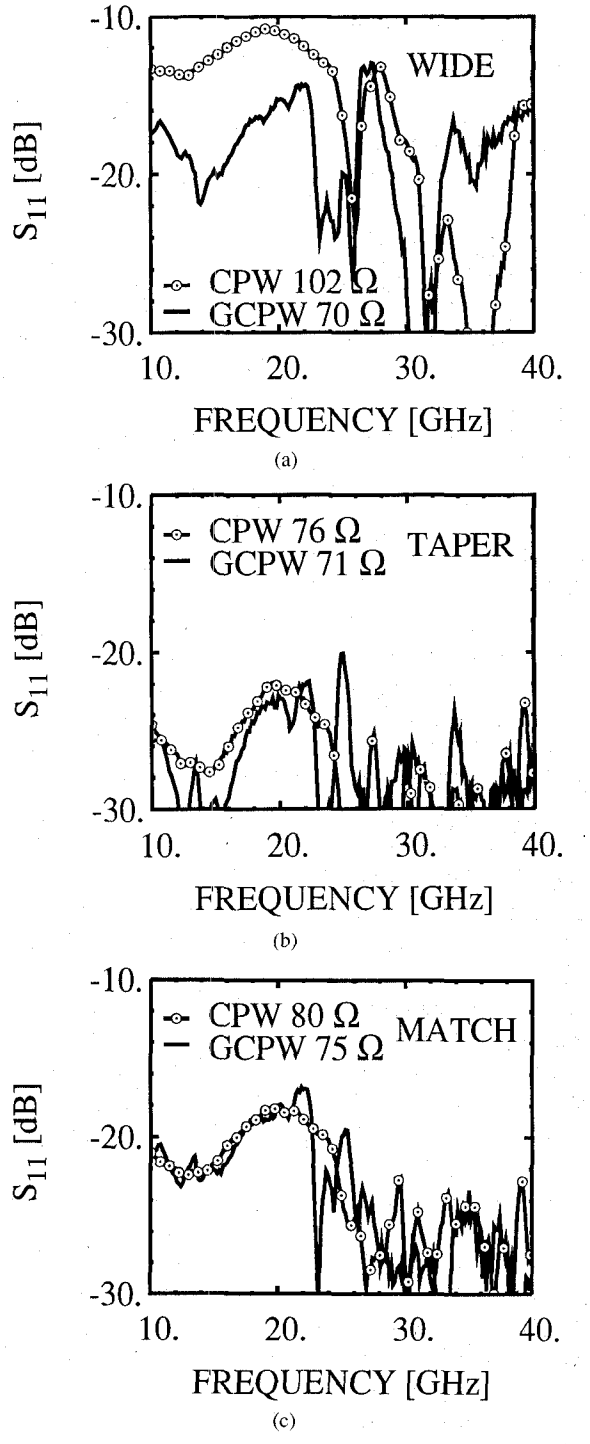

Fig. 10. Measured S_{11} for three transitions from 75 Ω microshield line to CPW and grounded CPW (GCPW). The plots are labeled to correspond to the designs in Fig. 9.

microshield and 'match' GCPW lines are only 5.8% and 6.2%, respectively, but for the 'wide' GCPW the change is 31%. The field mismatch is clearly reflected in the data, which shows that $S_{11,match}$ is 4-6 dB lower than $S_{11,wide}$ across the entire band.

Additional transitions were tested which have smaller geometries for both the microshield and GCPW lines than those in Fig. 9, and are therefore more appropriate for compact circuit configurations. The performance for two of the designs

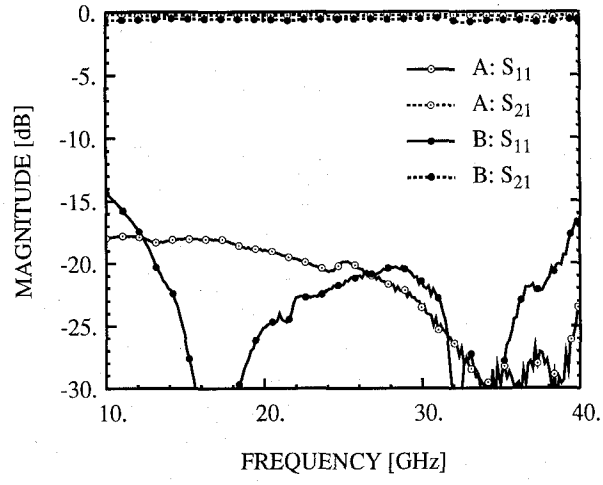

Fig. 11. Measured scattering parameters for two transitions from 75 Ω microshield line to grounded CPW (GCPW). The center conductor width (S) and slot width (W) for the microshield are 250 and 25, respectively. In curve A, the GCPW dimensions are $S = 50$, $W = 125$, and the length of the line is $L = 1460$. In curve B, the GCPW dimensions are $S = 30$, $W = 80$, and $S = 3500$. All dimensions are in microns.

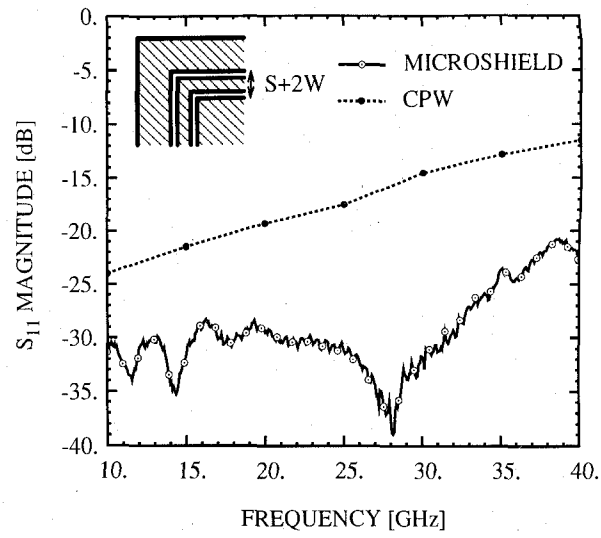

Fig. 12. Measured performance of right-angle bends fabricated using a microshield line and a CPW line on GaAs. The CPW bend has $S = 39$, $W = 24$, $H = 90$ and uses 2-μm-high air-bridges on each side of the bend [24]. The microshield line has $S = 250$, $W = 25$, and $H = 350$. All dimensions are in microns.

is shown in Fig. 11. These circuits were measured using the modified probe-to-microshield transition (Fig. 4) and thus the data has much less structure than in the previous figure. The strong resonances occur at frequencies for which the length of the GCPW sections are multiples of $\lambda_{\text{eff}}/2$. Each transition has a reasonably low reflection across the entire band, and it is expected that a rigorous full-wave analysis could lead to further design improvements.

B. Right-Angle Bend

A very common circuit 'element' in millimeter-wave systems is the right-angle bend. This structure gains significance with increasing frequency due to the parasitic capacitance and inductance which are associated with the abrupt change in the field orientation. These problems, combined with the mode-conversion which can also occur, result in a high reflection of the incident power (large S_{11}). In microstrip form, the typical means of improving the return loss is to miter the outside corners of the signal line [23]. This approach is less effective for coplanar waveguide [24], and alternative approaches such as air-bridges and dielectric overlays are adopted [25]. Both of these techniques are meant to offset the effects of different electrical path lengths along the two slots. Without this type of compensation, the asymmetry of the CPW right-angle bend will lead to excitation of the unwanted slot-line, or even, mode.

Many of the problems inherent to bends which are printed on conventional CPW-line can be minimized with the microshield geometry. The absence of the high dielectric constant material has two important effects: it leads to a reduction in the parasitic capacitance and, for a fixed physical size, it reduces the difference in electrical path lengths through the two slots. It has also been demonstrated that the even and odd mode propagation velocities are much closer on a membrane-supported line than on GaAs [5]. Therefore, in the event of even mode excitation, less signal degradation will occur with the microshield line. Finally, the shielding cavity provides continuous ground plane equalization without introducing additional discontinuities, unlike the conventional air-bridges used for CPW.

A comparison between the measured performance of a 75-Ω microshield-line bend and a 50-Ω CPW-line bend on GaAs [24] is shown in Fig. 12. The microshield bend has an S_{11} which is at least 8 dB lower over the 10–40 GHz band. Although data for a CPW bend similar to the microshield design could not be found, the comparison is justified since the small dimensions of the CPW bend result in an electrical path length difference through the slots which is less than half that in the microshield bend. Even when the lower ground plane was removed and the microshield bend was mounted on a styrofoam block, the S_{11} stayed below -20 dB, indicating that degradation due to the slot-line mode is minimal. The noise in the data below 18 GHz is due to calibration error.

C. Open-End and Short-End Series Stub

Another common coplanar waveguide component is the open-end series stub, which was previously analyzed by Dib *et al.* [6]. The passband resonance of the stub occurs when the mean length is $\lambda_{\text{eff}}/4$, and the associated radiation loss $(1 - |S_{11}|^2 - |S_{21}|^2)$ is very low due to the location of the stub within the center conductor. The stop-band resonance occurs when the stub length is $\lambda_{\text{eff}}/2$ and is considerably stronger than the passband resonance, resulting in higher radiation losses.

To demonstrate the stub characteristics, a comparison between measured and theoretical results for a typical design is given in Fig. 13. This stub has a narrower 3-dB bandwidth than a stub with similar transverse dimensions printed on silicon [26]. The theoretical data, which are in good agreement with the measured results, extend out to 70 GHz in order to show the stop-band response. Since the attenuation in the measured circuit is dominated by conductor loss, the radiation loss is calculated using the theoretical scattering parameters. Small

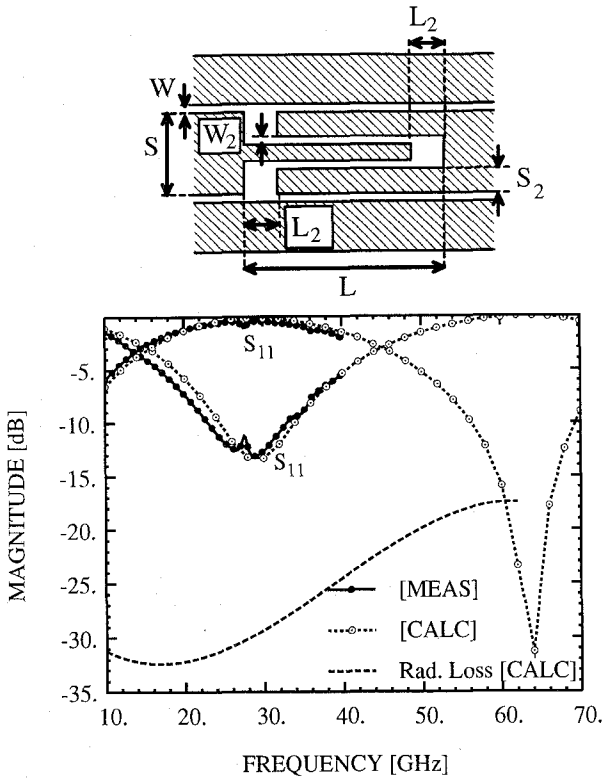

Fig. 13. Measured and calculated S-parameters for a microshield open-end series stub. The stub dimensions are $L = 2500$, $L_2 = 200$, $S = 250$, $S_2 = 80$, $W = 25$, and $W_2 = 25$. All dimensions are in microns.

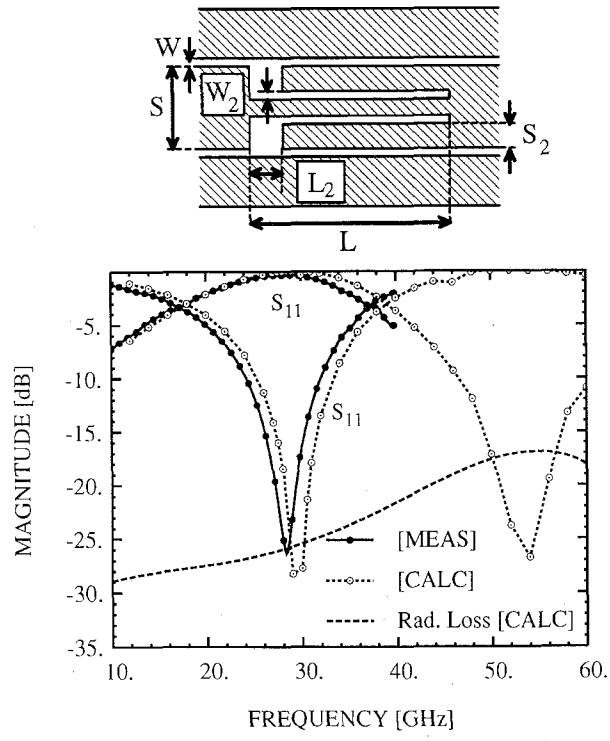

Fig. 14. Measured and calculated S-parameters for a microshield short-end series stub. The stub dimensions are $L = 2500$, $L_2 = 200$, $S = 250$, $S_2 = 80$, $W = 25$, and $W_2 = 25$. All dimensions are in microns.

errors in the numerical results caused erratic behavior of the radiation loss above 60 GHz, however, and these results are not shown. Also, the shift in the predicted frequency response is believed to result partly from using an inaccurate value for the effective dielectric constant (refer to Section I), as the slot widths in the actual circuit were 3–5 μm smaller than expected due to fabrication problems. As presented in Section IV, this causes $\epsilon_{r,\text{eff}}$ to increase and therefore reduces the resonant frequency.

D. Short-End Series Stub

The short-end series stub, like the open-end stub, is useful for a variety of circuits including bandstop filters, pin diode switches and attenuators, and has been reported by several authors [6], [27], [28]. The geometry offers the same advantages of compactness and low radiation loss. Unlike the open-end version, however, it has a much wider 3-dB bandwidth than a comparable stub printed on alumina or GaAs [26] (roughly 70% compared to 35%). The performance for a typical design which is $\lambda_{\text{eff}}/4$ at ≈ 30 GHz, along with results obtained from the full-wave analysis, are shown in Fig. 14. The shift in the frequency response is similar to the one in Fig. 13 and carries the same explanation.

E. Lowpass Filters

The stepped-impedance approach to lowpass filter design is a relatively easy technique to use, and it is well suited for applications which do not require a sharp roll-off in the insertion loss. Often, however, filter specifications call for high rejection over multiple-octave bandwidths, a requirement which may be difficult to meet using conventional substrate-supported lines due to the propagation of higher order modes. Thus the very broad, single-mode bandwidth of the microshield line can provide superior filter performance in this respect. In addition, the absence of the dielectric-related loss mechanisms, both attenuation and parasitic radiation, results in very low passband insertion loss.

Stepped-impedance filters using 5, 7, and 9 sections have been designed and tested. Some of the results were previously presented in [3], where it was shown that the measured performance compared very well with ideal transmission line theory, as a result of the pure TEM nature of the microshield propagating mode. In Fig. 15, the measured data for a 5-section, 0.5-dB ripple Chebyshev filter is compared with results from the full-wave analysis described in Section I. The rejection is greater than 20 dB up to 75 GHz, which is about 1.5 octaves above the 3-dB point at 26 GHz. Also, the measured S_{21} is between 0.25 and 0.9 dB from 10–23 GHz. This is very close to the 0.5-dB ripple design specification, and indicates that the attenuation is approximately 0.3 dB greater than predicted in the ideal, lossless model. The discrepancy between the measured and calculated data may be explained by the noise in the calibration (see Fig. 4) and the necessity to model this circuit with a single effective dielectric constant as discussed in Sections I and IV, even though the low- and high-impedance sections have drastically different slot widths.

As mentioned previously, a short-end series stub can be utilized to make circuits such as bandstop filters by cascading multiple stubs in series. It is also possible to take advantage of

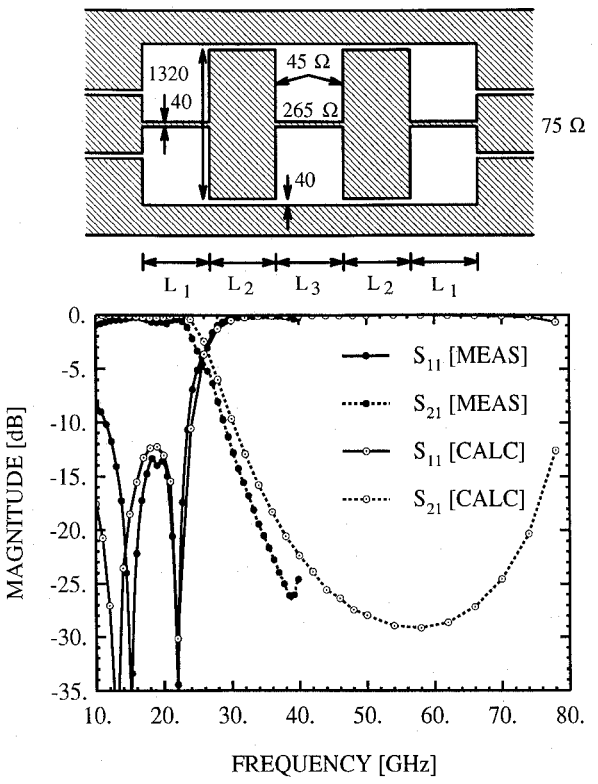

Fig. 15. Measured and calculated S-parameters for a microshield lowpass filter. The lengths of the different sections are $L_1 = 745$, $L_2 = 1200$, and $L_3 = 1189$. All dimensions are in microns.

the broad bandwidth of this stub to design high performance lowpass filters. One example is the addition of a short-end stub onto the end of the stepped-impedance lowpass filter described above. The stub has a length of 940 μm, with other dimensions identical to those listed in Fig. 14, and resonates around 90 GHz. By comparing the theoretical performance of this new filter in Fig. 16 to the performance without the stub in Fig. 15, it is clear that there is a significant improvement in the stopband of the filter. Another example is a very compact, easy to design lowpass/bandstop filter with a corner frequency of 40 GHz, which is simply the series combination of two 90 GHz stubs. This design has a total length of only 1.98 mm, using a 100 μm spacing between the stubs, and thus would have very low conductor loss along with the low radiation loss. The predicted performance is shown in Fig. 17.

F. Low-Loss Bandpass Filters

By cascading multiple open-end stubs in series, it is quite simple to realize a bandpass response with high out-of-band rejection and low loss. A three-section design was fabricated using the stub dimensions given in Fig. 13, with each section separated by 150 μm. The measured response, shown in Fig. 18, has an insertion loss of only 1.0 dB from 22–32 GHz, which is competitive with the best waveguide bandpass filters using suspended stripline. The performance of this microshield filter could be further improved using thicker metallization[3] or larger slot widths to minimize the conductor

[3] All circuits fabricated in this study had a metallization thickness of 1 μm.

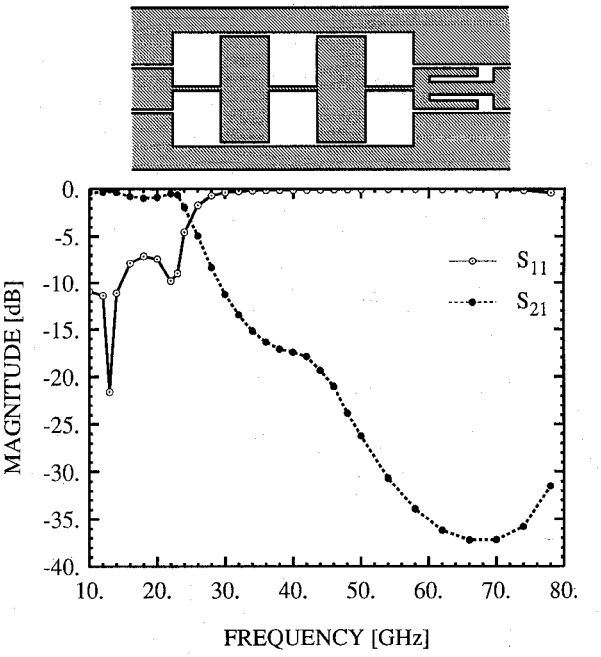

Fig. 16. Theoretical performance of the filter shown in Fig. 15 with a 90-GHz short-end series stub attached.

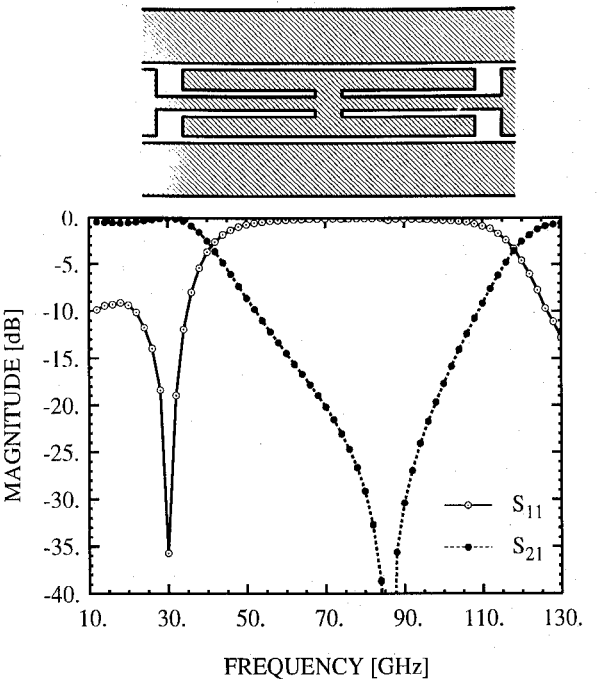

Fig. 17. Theoretical performance of two 90-GHz short-end series stubs (symmetric configuration).

loss. The calculated data is generated by using the scattering parameters found from the full-wave analysis of a single stub and treating the filter as three non-coupled elements in series. The agreement between the measured and calculated performance is quite good and indicates that there is very little electromagnetic coupling between the stubs, even though the stub separation is only 150 μm. The response of the filter can also be modeled almost exactly by cascading the *measured* results for a single stub, and this approach accurately predicts the 1.0 dB insertion loss.

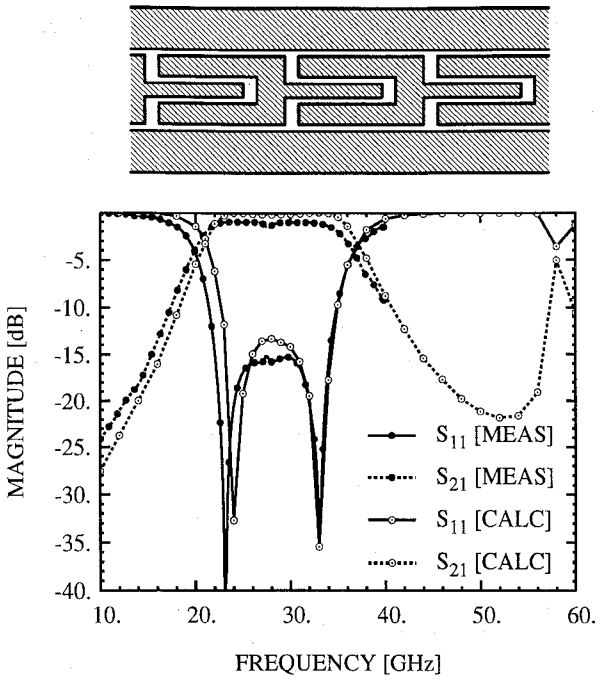

Fig. 18. Measured and calculated S-parameters for a microshield bandpass filter that consists of three open-end series stubs (Fig. 13).

VI. Conclusion

This paper presents a comprehensive introduction to the microshield transmission line and several passive circuit components. The measured performance from 10–40 GHz is very good and in certain cases superior to the performance which is characteristic of conventional coplanar waveguide circuits. Clearly, there are differences between the microshield line and a substrate-supported line, including larger circuit dimensions due to the low dielectric constant and the use of the thin dielectric membrane. At the same time, however, there are the advantages of having very broad-band TEM operation, a wide range of characteristic impedance, no requirement for air-bridges, and the possibility of using much thicker substrates at higher frequencies without the need for mechanical thinning. At submillimeter wavelengths, furthermore, the larger electrical size could simplify fabrication. Thus, the microshield line shows significant potential for high-performance millimeter wave applications, and is a strong candidate for submillimeter wave designs.

Acknowledgment

The authors thank Ms. Rhonda Franklin Drayton (UoM) and Mr. George E. Ponchak (NASA-Lewis/UoM) for their valuable discussions and considerable help in making the measurements, and Dr. Nihad Dib (UoM) for his expert help in the theoretical analysis.

References

[1] N. I. Dib, W. P. Harokopus, L. P. Katehi, C. C. Ling, and G. M. Rebeiz, "Study of a novel planar transmission line," in *1991 IEEE MTT-S Dig.*, Boston, pp. 623–626.

[2] N. I. Dib and L. P. Katehi, "Impedance calculation for the microshield line," *IEEE Microwave and Guided Wave Lett.*, vol. 2, no. 10, pp. 406–408, Oct., 1992.

[3] T. M. Weller, G. M. Rebeiz, and L. P. Katehi, "Experimental results on microshield line circuits," in *1993 IEEE MTT-S Dig.*, pp. 827–830.

[4] T. M. Weller, L. P. Katehi, G. M. Rebeiz, H. J. Cheng, and J. F. Whitaker, "Fabrication and characterization of microshield circuits," in *Proc. 4th Int. Symp. Terahertz Tech.*, University of California at Los Angeles, Los Angeles, CA, 1993, pp. 223–237.

[5] H. J. Cheng, J. F. Whitaker, T. M. Weller, and L. P. Katehi, "Terahertz-bandwidth characterization of coplanar waveguide on dielectric membrane via time-domain electro-optic sampling," in *1994 IEEE MTT-S Dig.*, pp. 477–480.

[6] N. I. Dib, L. P. Katehi, G. E. Ponchak, and R. N. Simons, "Theoretical and experimental characterization of coplanar waveguide discontinuities for filter applications," *IEEE Trans. Microwave Theory Tech.*, vol. MTT-39, no. 5, pp. 873882, May, 1991.

[7] G. F. Engen and C. A. Hoer, "Thru-reflect-line: An improved technique for calibrating the dual six-port automatic network analyzer," *IEEE Trans. Microwave Theory Tech.*, vol. MTT-27, no. 12, pp. 987–993, Dec., 1979.

[8] M. Tsuji, H. Shigesawa, and A. A. Oliner, "New interesting leakage behavior on coplanar waveguides of finite and infinite widths," in *1991 IEEE MTT-S Dig.*, pp. 563–566.

[9] H. Shigesawa, M. Tsuji, and A. A. Oliner, "Conductor-backed slot line and coplanar waveguide: Dangers and full-wave analyses," in *1988 IEEE MTT-S Dig.*, pp. 199–202.

[10] M. A. Magerko, L. Fan, and K. Chang, "Multiple dielectric structures to eliminate moding problems in conductor-backed coplanar waveguide MICs," *IEEE Microwave and Guided Wave Lett.*, vol. 2, no. 6, pp. 257–259, June, 1992.

[11] R. W. Jackson, "Mode conversion due to discontinuities in modified grounded coplanar waveguide," in *1988 IEEE MTT-S Dig.*, pp. 203–206.

[12] L. Wen-Teng, C-K. C. Tzuang, S-T. Peng, C-C. Chang, J-W. Huang, and C-C Tien, "Resonant phenomena in conductor-backed coplanar waveguide (CBCPW)," in *1993 IEEE MTT-S Dig.*, 1993, pp. 1199–1202.

[13] M. Riaziat, I. J. Feng, R. Majidi-Ahy, and B. A. Auld, "Single-mode operation of coplanar waveguides," *Electron. Lett.*, vol. 23, no. 24, pp. 1281–1283, Nov. 19, 1987.

[14] M. Riaziat, I. J. Feng, and R. Majidi-Ahy, "Propagation modes and dispersion characteristics of coplanar waveguides," *IEEE Trans. Microwave Theory Tech.*, vol. MTT-38, no. 3, pp. 245–251, Mar., 1990.

[15] E. M. Godshalk, "Generation and observation of surface waves on dielectric slabs and coplanar structures," in *1993 IEEE MTT-S Dig.*, pp. 923–926.

[16] W. H. Haydl, W. Heinrich, R. Bosch, M. Schlechtweg, P. Tasker, and J. Braunstein, "Design data for millimeter wave coplanar circuits," in *1993 European Microwave Conf.*, pp. 223–228.

[17] R. W. Jackson, "Considerations in the Use of Coplanar Waveguide For Millimeter-Wave Integrated Circuits," *IEEE Trans. Microwave Theory Tech.*, vol. MTT-34, no. 12, pp. 1450–1456, Dec., 1986.

[18] M. Zhang, C. Wu, K. Wu, and J. Litva, "Losses in GaAs Microstrip and Coplanar Waveguide," in *1992 IEEE MTT-S Dig.*, pp. 971–974.

[19] W. H. Haydl, J. Braunstein, T. Kitazawa, M. Schlechtweg, P. Tasker, and L. F. Eastman, "Attenuation of millimeterwave coplanar lines on gallium arsenide and indium phosphide Over the Range 1-60 GHz," in *1992 IEEE MTT-S Dig.*, pp. 349–352.

[20] W. J. Getsinger, "End-effects in quasi-TEM transmission lines," *IEEE Trans. Microwave Theory Tech.*, vol. MTT-41, no. 4, pp. 666–672, Apr., 1993.

[21] K. Beilenhoff, H. Klingbeil, W. Heinrich, and H. Hartnagel, "Open and short circuits in coplanar MMIC's," *IEEE Trans. Microwave Theory Tech.*, vol. MTT-41, no. 9, pp. 1534–1537, Sept., 1993.

[22] J. Machac and W. Menzel, "On the design of waveguide-to-microstrip and waveguide-to-coplanar line transitions," in *Proc. 23rd Euro. Microwave Conf.*, pp. 615–616.

[23] R. Chadha and K. C. Gupta, "Compensation of discontinuities in planar transmission lines," *IEEE Trans. Microwave Theory Tech.*, vol. MTT-30, no. 12, pp. 2151–2156, Dec., 1982.

[24] A. A. Q. Omar, "An accurate solution of 3-D coplanar waveguide circuits," Ph.D. thesis, University of Waterloo, Waterloo, Ontario, Canada, 1993.

[25] R. N. Simons and G. E. Ponchak, "Modeling of some coplanar waveguide discontinuities," *IEEE Trans. Microwave Theory Tech.*, vol. MTT-36, pp. 1796–1803, Dec., 1988.

[26] N. I. Dib, "Theoretical characterization of coplanar waveguide transmission lines and discontinuities," Ph. D. thesis, University of Michigan, Ann Arbor, MI, 1992.

[27] A. K. Sharma and H. Wang, "Experimental models of series and shunt elements in coplanar MMICs," in *1992 IEEE MTT-S Dig.*, pp. 1349–1352.
[28] P. A. R. Holder, "X-band microwave integrated circuits using slotline and coplanar waveguide," *Radio and Electron. Engineer*, vol. 48, no. 1/2, pp. 38–42, Jan./Feb. 1978.
[29] W. Menzel, "Broadband filter circuits using an extended suspended substrate transmission line configuration," in *Proc. 22nd Euro. Microwave Conf.*, Aug. 24–27, 1992, pp. 459–463.

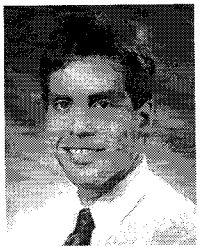

Thomas M. Weller received the B.S.E.E. and M.S.E.E. degrees from the University of Michigan, Ann Arbor, in 1988 and 1991, respectively. He is currently pursuing a Ph.D. in electrical engineering at the same university.

His present research involves micromachining applications for microwave circuits and numerical modeling in electromagnetics.

Linda P. B. Katehi (S'84–M'89–SM'94) received the B.S.E.E. degree from the National Technical University of Athens, Greece, in 1977 and the M.S.E.E. and Ph.D. degrees from the University of California, Los Angeles, in 1981 and 1984, respectively.

In September 1984 she joined the faculty of the EECS Department of the University of Michigan, Ann Arbor. Since then, she has been involved in the development, modeling, fabrication and experimental characterization of millimeter and near-millimeter wave monolithic circuits and antennas.

Dr. Katehi was been awarded the IEEE AP-S W. P. King Award in 1984, the IEEE AP-S S. A. Schelkunoff Award in 1985, the NSF Presidential Young Investigator Award and an URSI Young Scientist Fellowship in 1987, and the Humboldt Research Award in 1994. She is an associate editor of the IEEE TRANSACTIONS ON ANTENNAS AND PROPAGATION and *Radio Science*. She is a member of Sigma XI, URSI Commission D, and an elected member of the IEEE Antennas and Propagation Society Administrative Committee.

Gabriel M. Rebeiz (S'86–M'88–SM'93) was born in December 1964 in Beirut, Lebanon. He graduated in 1982 from the American University in Beirut with the B.E. (Honors) degree in electrical engineering, and earned his Ph.D. in electrical engineering from the California Institute of Technology in June 1988.

He joined the faculty of the University of Michigan in September 1988 and was promoted to associate professor in September 1992. He is the co-inventor (with Prof. Rutledge, Caltech) of the Integrated Horn Antenna. He is also the co-inventor of the Microshield Line (with Prof. Katehi, UM). His group has developed several key features of integrated millimeter-wave systems including low-noise planar room-temperature receivers, high-efficiency integrated antennas, and techniques for absolute power calibration. His group also demonstrated the first integrated millimeter-wave sub-system to date—a 94 GHz 4-channel monopulse tracking receiver with IF beam control. He also developed with Hughes Research Laboratories the highest frequency oscillator using a 3-terminal device in the world (220 GHz). His current research interests are in micromachining techniques in silicon and GaAs for microwave integrated circuits and components and in millimeter-wave imaging arrays. He spent eight weeks as a visiting professor at Chalmers University of Technology, Sweden. In 1992 and in 1993, he spent six weeks as a visiting professor at the Ecole Normale Superieur-France.

Dr. Rebeiz is the author of 51 papers published in refereed journals and 84 papers presented in national and international conferences. Together with his students, he is the winner of best paper awards in JINA'90, and in the IEEE-MTT'92, IEEE-AP'92, and IEEE-MTT'94. He received the National Science Foundation Presidential Young Investigator Award in 1991. He also received the URSI International Isaac Koga Gold Medal Award for Outstanding Research in August 1993. He is a member of URSI-Commission D.